PAPER

Check for updates

An isochoric optical platform for interrogation of aqueous glass formation processes†

Soheil Kavian, [a] Ronald Sellers,[a] Carla Berrospe-Rodriguez,[a] Crysthal Alvarez, [a] Fernanda D. Velasco,[a] Hunter B. Smith,[a] Guillermo Aguilar[ab] and Matthew J. Powell-Palm*[abc]

Aqueous vitrification (glass formation) processes are integral to modern cryopreservation, but experimental methods by which to study them are limited, particularly at the mL volume scales relevant to many biomedical applications. Here, we introduce an inexpensive custom optical platform, the isochoric vitrification cryo-macroscope (or "isovitriscope"), to supplement standard techniques with new qualitative and quantitative data streams. The platform consists of an LED light source, a isochoric (constant-volume) chamber with sapphire optical windows, and a camera, which can operate in two modes. One mode enables sharp visual observation of the glass transition and other low-temperature physical processes, including cracking, annealing, ice and hydrate crystallization, cavity formation, melting, *etc.* The other mode enables tracking of the optical temperature-evolution of the system *via* recorded light intensity, which we demonstrate may be used to measure the onset glass transition temperature with accuracy similar to differential scanning calorimetry (DSC), and to identify the temperature coordinates of other phase change events. The isovitriscope thus offers a single device combining the phenomenological insight of conventional visual inspection with the quantitative insight of techniques like calorimetry, at the >1 mL volume scales increasingly relevant to cryopreservation applications. To demonstrate uses of the isochoric optical platform, we herein conduct a series of observational studies examining the rich multi-phase phenomena at play during isochoric vitrification of binary cryoprotectant solutions; the effect of surface wettabilities on crack formation in the glassy state; the analogy between differential calorimetric and optical analysis; and more. In summary, the isochoric vitrification cryo-macroscope, or isovitriscope, adds a valuable new tool for the study of aqueous vitrification processes.

Introduction

Glass formation or vitrification of aqueous systems is essential to a range of biological and biomedical applications, ranging from the stabilization of samples for cryo-electron microscopy[1] to the preservation of complex tissues and organs for transplantation purposes.[2–4] However, achieving aqueous glass formation absent the growth of other phases (for example, crystalline ice) at solution concentrations tolerable to biological matter of interest has proven a constant technological challenge for the past several decades. This is abetted by a limited understanding of the glass transition as a fundamental process,[5,6] limited cryogenic-temperature thermophysical data on solutes and solutions of interest,[7] and a limited array of broadly accessible techniques by which to interrogate the process.

Glass transition phenomena of interest to biological applications are typically interrogated by two central techniques: differential scanning calorimetry (DSC)[8] and visual inspection.[9,10] DSC provides quantitative heatflow data from which the temperature coordinates of various thermal events may be measured, including the glass transition itself, ice nucleation upon cooling, ice nucleation upon warming, *etc.* However, the capacity of the technique to provide information relevant to cryobiological applications is limited in two key ways. First, the volume scale of DSC samples (∼µL) is orders of magnitude different than the scales relevant to many biological applications, which currently range from µL (ref. 11) to mL,[12] and are fast approaching L.[13] This mismatch makes it difficult to evaluate how volume-dependent phase change behaviors observed in DSC (such as ice nucleation[14]) might scale to practical systems of interest, though significant recent efforts have sought to address this issue through statistical kinetics approaches.[14,15] Second, calorimetry techniques are broadly insensitive to phase change phenomena without large thermal signatures (*i.e.* those whose

aJ. Mike Walker '66 Department of Mechanical Engineering, Texas A&M University, College Station, TX, 77843, USA. E-mail: powellpalm@tamu.edu

bDepartment of Materials Science & Engineering, Texas A&M University, College Station, TX, 77843, USA

cDepartment of Biomedical Engineering, Texas A&M University, College Station, TX, 77843, USA

† Electronic supplementary information (ESI) available. See DOI: https://doi.org/10.1039/d4ra03530e

latent heat contributions to the heat flow are of the same order or smaller than the sensible heat contributions of the liquid), making it difficult to observe processes that involve relatively small phase fractions, such as the initial growth of ice clusters in a viscous solution upon re-warming from the glass transition. Visual inspection, conversely, may be applied to some degree at most volume scales of interest, and may enable detection of phenomena that do not produce large thermal signals, but is otherwise acutely limited by its qualitative nature.

In this work, we seek to combine the quantitative strength of calorimetry with the observational granularity and volumetric flexibility of visual inspection into a single, inexpensive, high-throughput technique, in order to enhance the toolkit with which aqueous vitrification may be readily studied. To achieve this, we introduce the "isovitriscope", an isochoric (constant-volume) cryo-macroscope platform that leverages relative changes in the optical properties of aqueous materials upon vitrification process to measure phase transition temperatures, while enabling high-resolution and high-repeatability visual observation of the phenomena at play.

Across three classical cryoprotectant solutions, we demonstrate through proof-of-concept experiments that the isovitriscope, which is constructable for <$500 USD, achieves accuracy similar to DSC in identifying the onset glass transition temperature (DSC cost ∼$5000 to $150,000 USD), while providing significant additional qualitative and semi-quantitative information on various physical phenomena at play. These include glass cracking and annealing, ice and hydrate crystallization, eutectic nucleation and growth, and cavity formation. These phenomena often prove difficult or impossible to interrogate using calorimetric techniques, because (1) several require optical data streams to be observable (*e.g.* cracking, cavity formation); (2) several require bulk (mL-scale) sample volumes to be observable on laboratory time scales (*e.g.* nucleation of eutectic phases from viscous liquids, cavity formation); and (3) several may not produce sufficiently large thermal signatures to be detectable at high signal-to-noise confidence using calorimetric techniques (*e.g.* crack annealing, cavity formation, limited hydrate crystallization).

Furthermore, by integrating sapphire windows into a metallic isochoric chamber suited for submersion in liquid nitrogen, the isovitriscope enables the first (to our knowledge) visual observation of the aqueous vitrification process under isochoric conditions, which has been suggested to be capable of exhibiting a wealth of complex multiphysics behaviors,[16–18] many of which we are able to observe directly. While this work is intended as a proof-of-concept for the platform and technique, we suggest that even the simple form of the isovitriscope presented here may prove of significant use to laboratories investigating the rich complexities of the aqueous vitrification process.

Isovitriscope: design and operation

Advantages of isochoric systems for studying low-temperature aqueous phase change phenomena

Isochoric (constant-volume or volumetrically confined) conditions provide a number of advantages to the study of glass formation in aqueous samples. First, it has been shown variously that through a number of thermodynamic and kinetic mechanisms, rigid confinement of an aqueous sample can allay ice formation in bulk volume samples, *i.e.* enhance supercooling and ease the achievement of glass formation without (or with less) crystallization.[12,19–21] Second, the thermodynamic isolation from the outside environment that isochoric conditions provide enables a high degree of control over the boundary conditions of the liquid, facilitating good repeatability and eliminating the confounding effects of the liquid–atmosphere interface.[21] Multiple works have shown a reduction in the spread of ice nucleation temperatures under isochoric conditions, as opposed to open conditions, demonstrating this repeatability.[21,22] Finally, under isochoric conditions, every surface of the liquid sample is in adhesive contact with a solid surface which reduces liquid surface deformation that may confound optical observations.

Isochoric chamber design

The complete isochoric vitrification macroscope ("isovitriscope") platform is shown schematically in Fig. 1a, and the isochoric chamber around which the platform is built is detailed in Fig. 1b and c.

The body and lids of this chamber are constructed from Type II anodized Al-7075, selected for its excellent machinability, affordability, and thermal conductivity. The chamber holds a sample volume of 2 mL when sealed. The viewports are sapphire crystal disks, each 25.4 mm in diameter and 5 mm thick (Thorlabs WG31050), chosen for their combination of high thermal conductivity, high yield strength, and high optical transparency. Face-sealing PTFE O-rings (McMaster-Carr 9559K61) are mounted between the chamber body and the sapphire viewports to ensure a hermetic seal. Compression of the o-ring and retention of the sapphire is achieved by five M3 stainless steel bolts (per side) as shown in Fig. 1c. A slot of an approximately 1 mm-diameter point-thermocouple was machined in the center of the chamber's side, extending 12 mm into the wall (5 mm from the sample). When assembled, the isochoric chamber is capable of withstanding temperatures down to −200 °C, as well as pressures up to 200 MPa. While the vitrification processes investigated in this work do not produce positive pressures and pressure is not measured, future iterations of this device may easily incorporate pressure sensing, enabling more granular interrogation of the pressurized isochoric *freezing* process.

To avoid condensation during imaging at cryogenic temperatures, the chamber is first allowed to reach thermal equilibrium in liquid nitrogen (as described below). After this, the chamber is placed inside a custom-made PLA insulation sleeve with acrylic viewports, which can be seen surrounding the chamber in Fig. 1a. The sleeve not only prevents condensation but also helps achieve the slow warming rates that are necessary to observe many of the transient phase change phenomena of interest.

Optical platform

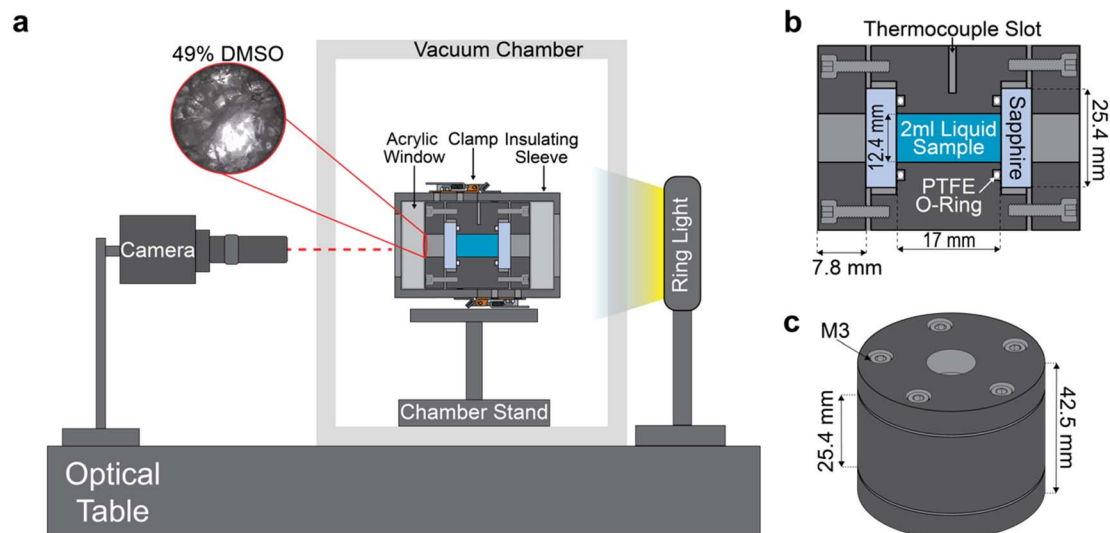The isovitriscope platform is mounted on a Vision Isostation optical table (Newport VIS3048-SG2-325A), which houses

Fig. 1 Isochoric vitrification cryo–macroscope (isovitriscope) platform. (a) Schematic representation of the isovitriscope. The isochoric chamber is first cooled to −196 °C in a liquid nitrogen bath, then transferred to a 3D-printed insulation shell and placed in an acrylic vacuum chamber to prevent condensation on the optical windows and enable repeatable warming rates. Optical data is recorded during the warming. (b) Cross-sectional view of the isochoric chamber. The body is machined from Al7075-T651, with a Type-II anodize. (c) Isometric view of the isochoric chamber.

a camera, vacuum chamber, and light source, as shown in Fig. 1a. We use a <$150 USD, USB 4k-resolution 30-FPS camera (ELP-USB4KHDR01) equipped with an inexpensive third-party lens (Waveshare Electronics) for a range of optical magnifications from 0.12× to 1.8×, with up to 100× digital zoom. We also employ a variable neutral density filter (K&F Nano X) to manually adjust the amount of light allowed into lens. This camera system is oriented in-line with the isochoric chamber, which is mounted on a custom stand within an acrylic vacuum case. The case helps prevent condensation on the on the viewports of the chamber during imaging. The system is lighted from behind by a <$30 USD 144-LED ring light which has an outer diameter of 95 mm and inner diameter of 61 mm (Bikani).

Vitrification and observation protocol

For each trial, 2 mL of aqueous solution is loaded into the chamber when positioned vertically (as shown in Fig. 1c). The sapphire viewport is placed atop the open face of the sample and the bolts are advanced to compress the o-ring, achieving a water-tight face seal. Care is taken to avoid introduction of air bubbles, dust, or other debris that may affect the nucleation, vitrification, or crack propagation processes of interest. After sealing, the thermocouple is inserted into the chamber wall slot and covered with thermal paste, temperature monitoring is initiated, and the chamber is plunged into a bath of liquid nitrogen.

In this work, in the interest of examining the effect of cooling rate on our optical metrology process, we examine two representative rates. The "fast" cooling rate ($\sim$−200 °C min^{-1}) is achieved by plunging the chamber as described above. The "slow" cooling rate ($\sim$−5 °C min^{-1}) is achieved by first placing

the chamber onto a 3D printed stand in a 500 mL borosilicate beaker (such that it is not in conductive contact with the glass), then submerging the beaker in liquid nitrogen. Once liquid nitrogen (LN2) temperature equilibration (−196 °C) is reached, the chamber is removed from the cooling bath and rapidly clamped into the 3D printed insulating shell. The insulated chamber assembly is then placed on a custom mount in the vacuum chamber and vacuum is drawn, preventing condensation and nitrogen vapor from obstructing the camera view and ensuring a sufficiently slow warming rate for high-fidelity observation ($\sim$5 °C min^{-1}). Representative temperature traces for both cooling/warming protocols are shown in ESI Fig. S2.†

Optical analysis techniques

To collect optical data during the glass transition, we employ two different techniques: dynamic light intensity (DLI) and constant light intensity (CLI) monitoring. In DLI monitoring, the source light intensity is continuously varied to allow sharp visual observation of the phenomena occurring during the warming process, including crack annealing, ice, hydrate, and eutectic crystallization processes, cavity-driven nucleation processes, *etc.* The CLI monitoring, which allows for the source light intensity to be maintained at a constant value and the intensity recorded by the camera, enables quantitative interrogation of the optical changes occurring in the sample with change in temperature.

Dynamic light intensity (DLI) monitoring

Fig. 2 provides a representative timelapse recorded using DLI monitoring after vitrification at a cooling rate of $\sim$−200 °C min^{-1}, shown in the glass transition temperature range for
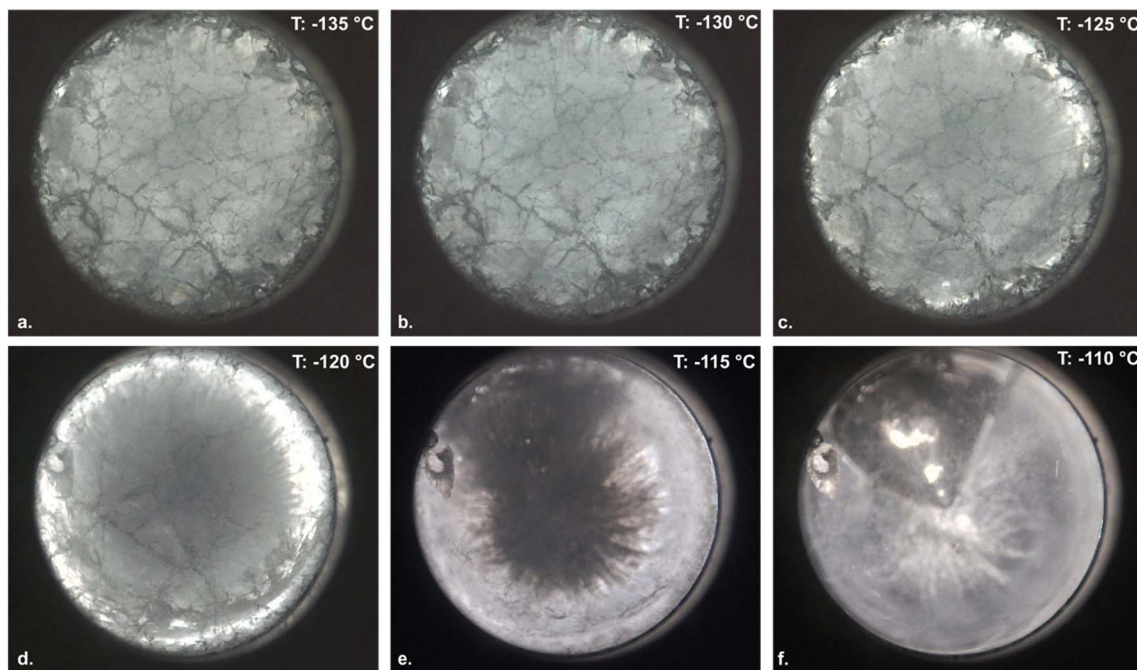
Fig. 2 Representative time-lapse images of the glass transition process upon warming in 49% DMSO. Images taken at chamber-wall temperatures of (a) −135 °C, (b) −130 °C, (c) −125 °C, (d) −120 °C, (e) −115 °C, (f) −110 °C. Source light intensity was adjusted manually in real time to enable consistent measured intensity at the camera (and thereby consistent visual contrast).

49% DMSO. The transition proceeds as expected, phenomeno-logically: at temperatures below the end of glass transition (∼−130 °C for 49% DMSO; Fig. 2b), a densely cracked solid glass is observed; as the glass enters the glass transition region, annealing of the cracks and emergence of the viscous liquid phase begins, proceeding the outer edges according to the radial temperature gradient imposed by warming from the external surfaces (Fig. 2b–f); and upon completion of the glass transition, a uniform liquid with a large vapor cavity is observed. This vapor cavity is characteristic of isochoric vitrification processes involving highly contractile solutions like 49% DMSO.[16,17]

It should be noted that the temperature marked in Fig. 2, which is recorded by thermocouple near the periphery of the sample, is obviously not representative of the entire sample, which experiences a significant temperature gradient during warming due to the low thermal diffusivity of the aqueous sample and its large (2 mL) volume. In the following sections we quantify these gradients using finite-element analysis, and account for them in our CLI quantitative optical analyses. However, for visual evaluation of glass formation phenomenology, the gradients should simply be noted. Additional representative images and videos of DLI monitoring of the warming process are provided in ESI Note 3, and in ESI Video 1† (49% DMSO, ∼200 °C min⁻¹ cooling rate), ESI Video 2† (79% glycerol, ∼200 °C min⁻¹ cooling rate), and ESI Video 3† (59% EG, ∼200 °C min⁻¹ cooling rate).

Phenomenology of glass formation and rewarming under isochoric conditions. While the vitrification phenomenology of ≥49% DMSO under isochoric conditions has been examined

previously by theory and X-ray computed tomography (CT),[16,17] the behaviors of many other solutions of common interest to cryobiology remain unexplored. Furthermore, many interesting multi-physics phenomena that may arise as a consequence of thermo-volumetric effects unique to confined systems have been suggested,[17,18] but never directly observed. Using DLI monitoring, we observe a host of such phenomena, displayed in Fig. 3 for solutions of ethylene glycol, DMSO, and glycerol.

Based on initial X-ray CT observations by Parker *et al.*,[17] Kavian & Powell-Palm[18] hypothesized that vapor cavities formed during isochoric vitrification due to solution contraction will provide a preferable environment for ice growth during cooling or re-warming, due to the heterogeneous nucleation capacity of liquid–gas interfaces[23] and the favorability of the low-pressure zone for ice crystal growth. In Fig. 3a–d, we observe this precise phenomenon during re-warming of a sample of 59% EG vitrified at ∼−5 °C min⁻¹. First, at temperatures beneath the glass transition temperature (∼−130 °C), a cracked glass with a column of contraction-induced vapor bubbles is observed. After the glass transition, the cracks anneal way and a uniform viscous liquid is observed, alongside interesting apparent shifts in color that warrant future spectral analysis. Note further that the vapor cavities present decrease somewhat in size, consistent with thermal expansion of the fluid. Next, at 40–50 °C above the glass transition temperature, many of the vapor cavities have collapsed, and ice is observed growing directly into the remaining large cavity, in support of the hypothesis of Kavian & Powell-Palm.[18] Finally, at 45–55 °C above the glass transition temperature, significant additional ice growth has filled the cavity, and a fine crystalline phase has nucleated in the bulk
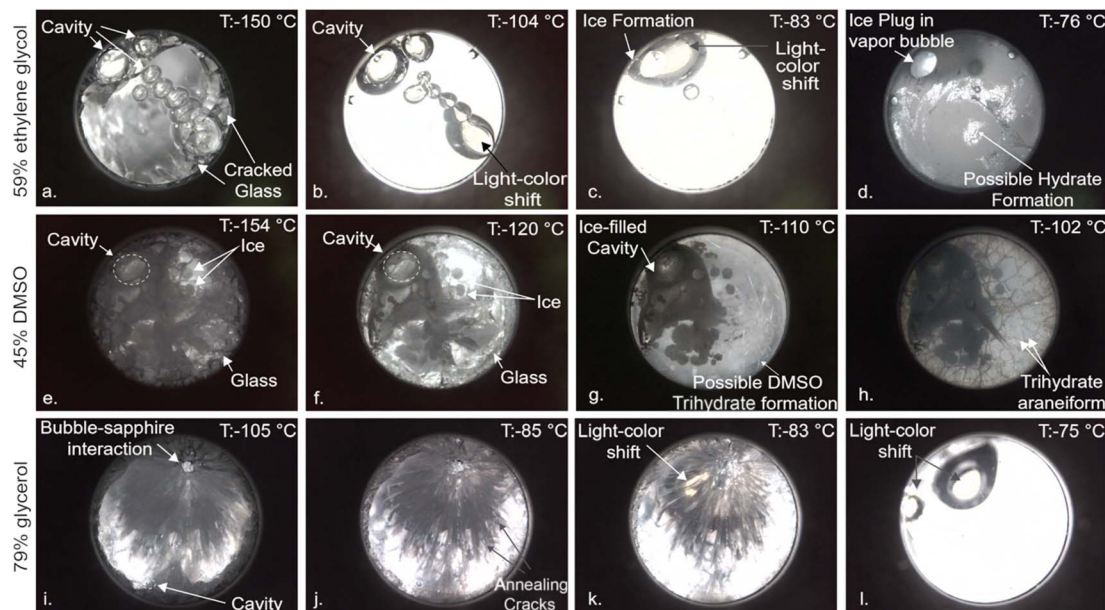
Fig. 3 Multi-phase multi-physics phenomena at play during isochoric vitrification processes in various solutions. (a–d) Time-lapse upon warming of 59% ethylene glycol cooled at ∼5 °C per minute, highlighting the noticeable shift in wavelength absorption with temperature, cavity formation and movement, initial ice formation within vapor cavities, and possible hydrate formation. (e–h) Time-lapse upon warming of 45% DMSO cooled at ∼200 °C min^{-1}, highlighting the simultaneous presence of glassy, crystalline, and vapor phases at cryogenic temperatures, and observation of a possible DMSO trihydrate araneiform. (i–l) 79% glycerol cooled at ∼5 °C min^{-1}, highlighting role of vapor cavities in localizing crack formation.

liquid, which based on the water–ethylene glycol phase diagram,[24] we hypothesize to be either ice, the monohydrate of ethylene glycol (EG-H20), or a combination of the two, given that these temperatures are beneath the ice-1 h – EG H20 eutectic temperature at this concentration.

Next, in Fig. 3e–h we examine a solution of 45% DMSO, a concentration less than the critical concentration for complete vitrification (generally taken to be 49% DMSO), cooled at ∼200 °C min^{-1}. At sub-T_g temperatures, we observe an intriguing multiphase combination of crystalline, glassy, and vapor phases, a configuration unique to isochoric vitrification that was also hypothesized previously to be possible. It is important to note that the cavity here was not present upon assembly of the chamber, but instead produced by tensioning and eventual cavitation or outgassing of the liquid upon thermal contraction under confinement.[16–18] At temperatures tens of degrees above the glass transition (Fig. 3e), ice has preferentially filled the vapor cavity, in addition to growing in small clusters in the bulk liquid. Finally, at temperatures 20–30 °C above the glass transition, a distinct crystalline araneiform is observed to form along the surface of the sapphire, which we hypothesize per the phase diagram[25] to be DMSO-trihydrate. As will be confirmed later in this work but should be easily intuited, the emergence of this alternate crystalline phase upon warming is virtually undetectable by DSC, given its miniscule volume (and thus latent heat signature). This phenomenon warrants significant further investigation by Raman spectroscopy or similar, in order to confirm the precise phase and to interrogate the nature of the araneiform structure.

Finally, in Fig. 3i–l we investigate a solution of 79% glycerol cooled at ∼5 °C min^{-1}, in which we observe local crack propagation (and ensuing annealing) concentrated around a large vapor cavity, consistent with understanding from thermomechanics that evolving liquid–cavity interface will likely represent the zone of maximum strain in the system.[26] Additionally, wavelength/color shifts (white to yellow) similar to those seen in 59% ethylene glycol are observed during and after the glass transition, possibly due to the significant changes in viscosity that accompany the glass transition region.

Compositional analysis using Raman spectroscopy. In order to further probe compositional aspects of these systems during warming, and in particular the potential formation of low-phase fraction hydrate phases that may not produce significant thermal signals, we also integrated the isovitriscope platform with a custom Raman spectroscopy system previously established in our lab[27] and repeated our cooling–warming protocol. The configuration is described in detail in ESI Note 5.†

Our analysis here will focus on Raman spectra from 2500 to 4000 cm^{-1}, where the water molecule exhibits strong Raman emission and phase transitions can be observed, but spectra from 200 to 4000 cm^{-1} are provided in ESI Note 5.† The room-temperature Raman spectra captured inside the isochoric chamber are shown in Fig. 4a. The typical stretching modes of glycerol, EG and DMSO, as well as the O–H stretching modes (orange dashed square) of the water molecule are observed as expected.

Upon warming process from the vitrified state, Raman spectra were obtained for each solution at various temperatures
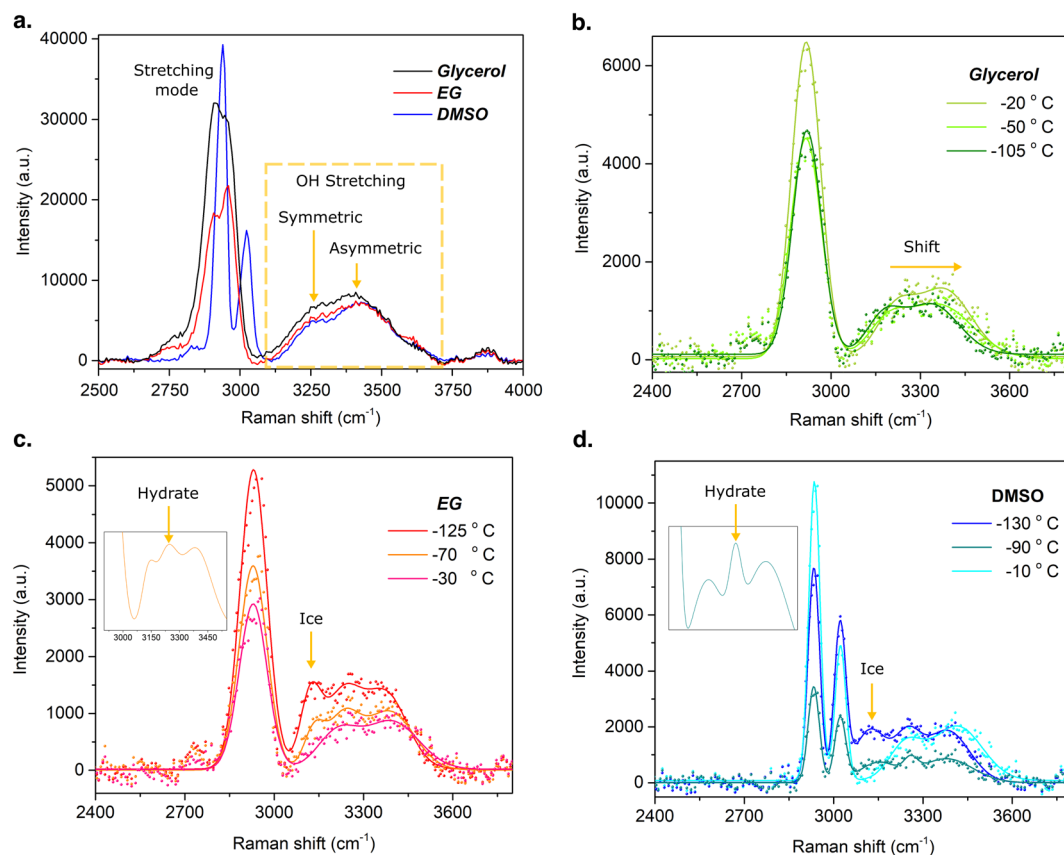
© 2024 The Author(s). Published by the Royal Society of Chemistry

Fig. 4 Raman spectroscopy during warming after isochoric vitrification. (a) Raman spectra from 2500 to 4000 cm^{-1} of 79% glycerol, 59% EG and 49% DMSO solutions at room temperature. The orange dashed square shows the O−H stretching modes for the water molecule. Upon warming from vitrification: (b) 79% glycerol, showing a right shift of the O−H stretching modes as temperature increasing. (c) 59% EG showing, showing ice nucleation and possible hydrate formation following the glass transition. (d) 49% DMSO, showing ice nucleation and possible hydrate formation following the glass transition.

(Fig. 4b–d). It is important to note that the spectrum and its corresponding temperature are average values acquired during warming, based on a total acquisition time of 2 minutes, with an integration time of 10 seconds and 12 iterations. The average warming rates recorded for each solution were 7.8 °C, 8.2 °C, and 6.3 °C per minute for DMSO, EG, and glycerol, respectively, and this acquisition time thus represents a temperature window of approximately 15 °C, the average value of which is reported for each curve in the figure. The spectra for 79% glycerol, represented in Fig. 4b, illustrates a right shift of the water OH stretching modes and an intensity magnitude increase of the asymmetric mode as temperature increases. These changes in the Raman spectra indicate the transition of the solution from the vitrified (−105 °C) to the liquid state (−50 °C, −20 °C). Note that there is no evidence of ice nucleation, in agreement with the *via* visual examination of the same system (Fig. 3i–l). Fig. 4c shows the spectra for 59% EG. Herein both ice formation (at ~3130 cm^{-1} (ref. 28)) and an additional phase (at ~3250 cm^{-1}), likely ethylene glycol monohydrate,[24] are observed at temperatures greater than approximately −130 °C, and return to the homogeneous liquid phase is confirmed at approximately −30 °C. Similarly to glycerol, the 59% EG shows a right shift of the O–H stretching mode of water as well as enhancement of the

asymmetric mode during warming through the glass transition. Fig. 4d shows the spectra for 49% DMSO, which also suggests the formation of ice upon warming. However, the emission at ~3130 cm^{-1} is significantly lower than observed for EG, suggesting a reduced phase fraction of ice in 49% DMSO. The formation of DMSO-trihydrate is also suggested by a peak observed at ~3262 cm^{-1},[29] as is shown in the inset image of Fig. 4d. These spectroscopic insights broadly support the observations drawn from Fig. 3 based purely on visual evaluation of the system, further highlighting the utility of the isovitriscope platform as a technologically-simple exploration tool for the study of low-temperature phase change processes.

Effect of solid–liquid surface interactions on crack behavior. Isochoric conditions provide the unique opportunity to dictate every surface interaction experienced by the liquid sample, and therefore the opportunity to interrogate the contribution of said surface interactions to various vitrification phenomena. To illustrate this point, we performed a simple set of experiments demonstrating the dominant role of surface hydrophobicity in crack development.

The isochoric chamber includes two key types of liquid–solid interface: the liquid–aluminum interface along the radial walls of the chamber and the liquid–sapphire interface at its ends.

The two solids at play are each mildly hydrophilic (as evidenced by water–solid contact angles of 60–90° (ref. 30 and 31)) and are assumed herein to provide broadly similar forces of solid–liquid adhesion. In order to determine whether the role of this adhesive force may be interrogated using the isovitriscope platform, in four experiments, we applied a commercial hydrophobic coating (RainX, water contact angle ~110° (ref. 32)) to either (1) none of the surfaces in contact with the liquid, (2) only the chamber walls, (3) only the sapphire windows, and (4) both the chamber walls and the sapphire windows (*i.e.* all surfaces in contact with the liquid).

We vitrified samples of the CVS1 coral preservation solution developed by Powell-Palm *et al.*[12] (chosen because of its role in recent applications and fundamental studies of isochoric vitrification[12,17]) under each of these combinations of hydrophilic and hydrophobic surfaces and observed crack morphology at the onset of warming, the results of which are displayed in Fig. 5.

For no surface treatment (or alternatively, for similar *hydrophilic* wall and window wettabilities), cracks appeared approximately uniform across the sample. When both surfaces were treated with RainX (similar *hydrophobic* wall and window wettabilities), similar uniformity was observed, albeit with perceptibly different (if difficult to qualify) appearance. However, when RainX was applied *only* to the chamber surface, cracking across the center of the field of view largely disappeared, instead stemming nigh-exclusively from the walls. When RainX was applied only to the sapphire windows conversely, cracking was once more observed throughout the image, consistent cracking stemming from the sapphire surface.

Fig. 5 suggests that manipulation of local solid–liquid adhesive forces (here by the use of hydrophobic *vs.* hydrophilic solid surfaces) can enable spatial control of where and how crack formation occurs, which could prove valuable in combatting thermal stress cracking during cryopreservation. This observation is conceptually consistent with the findings of Vispute *et al.* and Rabin,[26,33] who demonstrate that cracking in unconfined systems will generally proceed from the most mobile liquid surface (which is typically that surface interfacing with air), simply because that mobility enables higher strain in response to thermal contraction, and therefore higher stress upon rapid cooling. The role of solid–liquid interfacial interactions in thermal stress cracking warrants considerable further investigation, and highlights the potential for new areas of study using the present optical platform.

The results above in total provide an initial demonstration of the isovitriscope observational potential operating in (DLI) mode, wherein the light source is continuously adjusted to maintain optimal contrast for visual evaluation. Next, we will demonstrate the utility of (CLI) mode, wherein sharp visual observation is traded for quantitative information on the optical evolution of the system with temperature.

Constant light intensity (CLI) monitoring

While dynamic adjustment of the source light intensity is required to maintain good image contrast and facilitate detailed visual inspection, the isovitriscope may also be operated with a constant source light intensity. In this case, evolution of the optical properties of the system may be measured continuously as a function of temperature by simply analyzing the change in intensity recorded by the camera. We will demonstrate herein that this intensity change responds to phase change with a sensitivity similar to the thermal changes measured by DSC, similarly accurate measurement of the glass transition temperature.

General approach. The general intensity analysis approach is as follows. First, recorded temperature-tagged images are converted to grayscale. The pixel-wise intensity difference between a given grayscale image ($I_{current}$) and the first grayscale image in the sequence (I_{first}, corresponding to the lowest-temperature frame) is then computed. The average intensity difference for each image relative to the first image is then calculated according to the following formula:

$$\text{Average intensity difference} = \frac{1}{N} \sum_{i=1}^{N} \left(I_{current}(i) - I_{first}(i) \right)$$

where N represents the total number of pixels in the image, $I_{current}(i)$ is the intensity of the ith pixel in the current grayscale
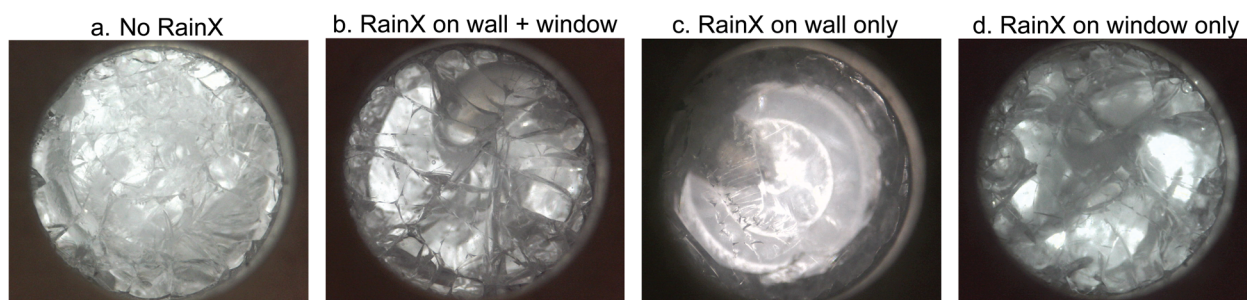

Fig. 5 Impact of relative surface wettability on crack formation during isochoric vitrification of the CVS1 solution. (a) Crack morphology with uncoated and similarly hydrophilic wall and window surfaces, (b) crack morphology with hydrophobic coating (RainX) on both wall and window surfaces, (c) crack morphology with hydrophobic coating on the chamber wall only, (d) crack morphology with hydrophobic coating on the sapphire window only. All images show the same solution composition, cooled at the same rate (~200 °C min^{-1}).

image, and $I_{first}(i)$ is the intensity of the ith pixel in the first grayscale image.

This procedure is then applied to the series of images comprising a full video of the warming process, indexed from the first image (when the sample has just been removed from liquid nitrogen and mounted on the optical platform) to the last image (at the end of the warming process).

Pixel selection for temperature accuracy. As mentioned previously, there exist large and apparent temperature gradients across the aqueous sample, driven by the low thermal diffusivity of organic aqueous solutions (especially at cryogenic temperatures)[34] and the large sample volume. As such, we anticipate that the temperature reported by the thermocouple, which is mounted in the aluminum wall of the chamber, 5 mm from the interface with the liquid sample, will reflect the true temperature of the sample only within a small radial distance from the wall–sample interface. In principle, in the context of our (CLI) analysis, if this radial distance can be quantified, a subset of the total pixel space for which the temperature is well known can be analyzed according to the approach above, guaranteeing accuracy of temperature.

In order to identify this radial distance of interest, a thermal finite element simulation was performed in ANSYS (simulation setup and assumptions detailed in ESI Note 1†), the results of which are shown in Fig. 6. For a DMSO-like solution assumed to be symmetrically warmed, Fig. 6a displays temperature transients at various radial distances from the wall of the chamber, and Fig. 6b shows a radial cross-section with temperature contours marked at a single time (the onset of the assumed glass transition). These results indicate that within an approximately 1 mm radial distance from the wall–sample interface, the sample temperature should vary by less than approximately 1 °C from the thermocouple measurement (throughout the warming process), whereas at the center of the chamber, the temperature may lag between 7 °C to 10 °C behind the thermocouple measurement. While different aqueous glass transitions of course have different associated latent heats and these simulations do not perfectly recapitulate the thermal evolution of the real sample, we conclude based on Fig. 6 that within 1 mm radial distance from the chamber wall, an accuracy of approximately ±1 °C may be presumed across solutions.
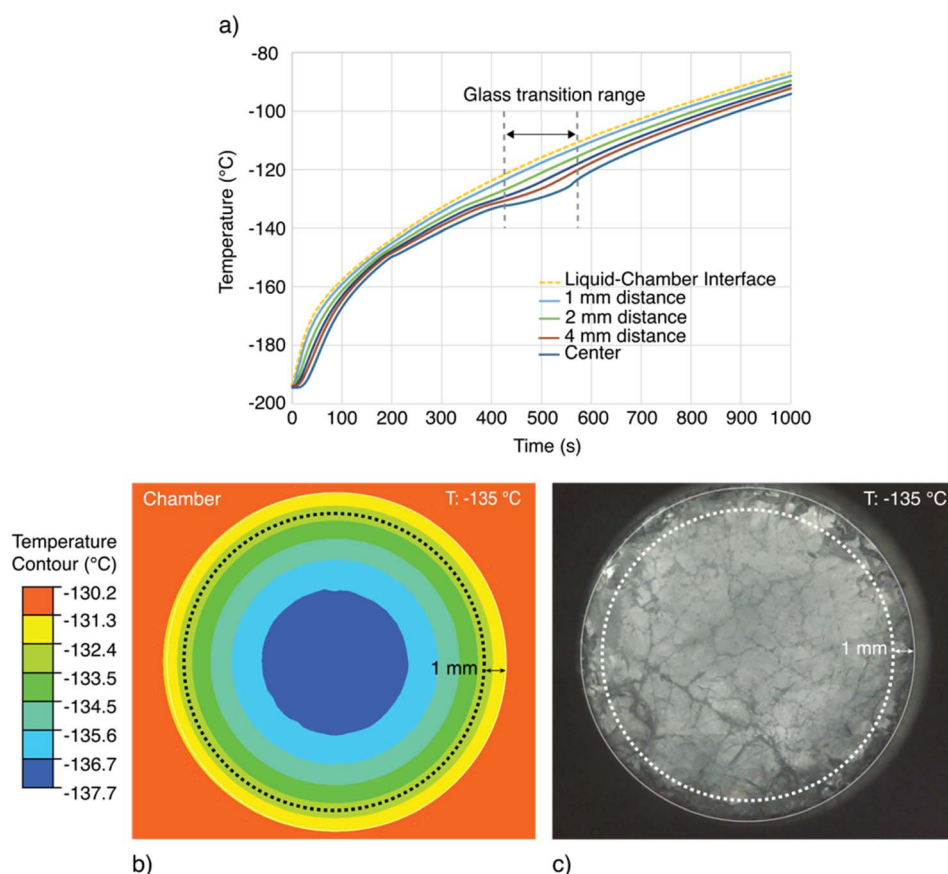

Fig. 6 Thermal analysis of the temperature lag between the wall-mounted thermocouple and the interior of the liquid sample. (a) Transient temperature evolution of the liquid sample at varying radial distances from the chamber wall, assuming the thermophysical properties of 49% DMSO. Simulation details in ESI Note 1.† (b) Temperature contour plot of the chamber interior in the glass transition range surrounding −130 °C. An approximately ~7 °C maximum temperature difference exists between the center of the liquid sample and the chamber wall wherein the thermocouple is embedded experimentally. Likewise, a maximum difference of approximately ~1 °C exists between the chamber and the contour 1 mm from the liquid–wall interface. (c) Depiction of the annular ring of visual data analyzed using the (CLI) method, for which an average temperature resolution of <1 °C can be guaranteed.

As such, in order to accurately map optical changes in the sample to temperature, we perform the pixel intensity analysis described above only on the annular ring of pixels within 1 mm of the wall–sample interface. This region is indicated on a representative image in Fig. 6b and c.

Results and validation against DSC. Representative pixel intensity analysis results are shown in Fig. 7a for slow warming ($\sim$5 °C min^{-1}) of solutions of 49% DMSO, 59% ethylene glycol, and 79% percent glycerol, vitrified at both slow ($\sim$5 °C min^{-1}) and fast ($\sim$200 °C min^{-1}) cooling rates. The general phenomenological behaviors of interest are labeled, and proceed broadly as follows. In the glassy region, the intensity remains largely consistent, increasing mildly and approximately linearly with temperature. Upon glass transition (and the many-orders-of-magnitude decrease in viscosity that accompany it) the intensity rises sharply, reflecting the enhanced transparency of the liquid phase relative to the amorphous solid phase. Thereafter the intensity remains relatively consistent, until (in the cases of DMSO and ethylene glycol) crystallization occurs, leading to a precipitous drop driven by the scattering of light by crystal-liquid boundaries. As warming continues, melting begins, leading the intensity to rise once more, until such time as the last solid crystals dissipate and the intensity curve flattens in the liquid phase. For reference and comparison, we also acquired DSC data for the same solutions at a 5 °C cooling/warming, and the same behaviors are labeled where discernible. All trials (isovitriscope and DSC alike) were performed in triplicate.

In order to extract a glass transition temperature from the pixel intensity data shown in Fig. 6, we apply a method similar to that used in DSC analysis, examining characteristic changes in the derivative of the signal. The glass transition of course occurs over a range of temperatures, and, per ASTM E1356-08, can be described by as many as six discrete values in that range, but for the purposes of illustration herein we target only the onset temperature of the glass transition (upon warming), as the field of cryobiology typically defines the process with a single representative temperature.[8] To extract this temperature, a function is developed (implemented in MATLAB 2023b), to detect the glass transition point on average intensity curves shown in Fig. 6a. Generally, the glass transition point is
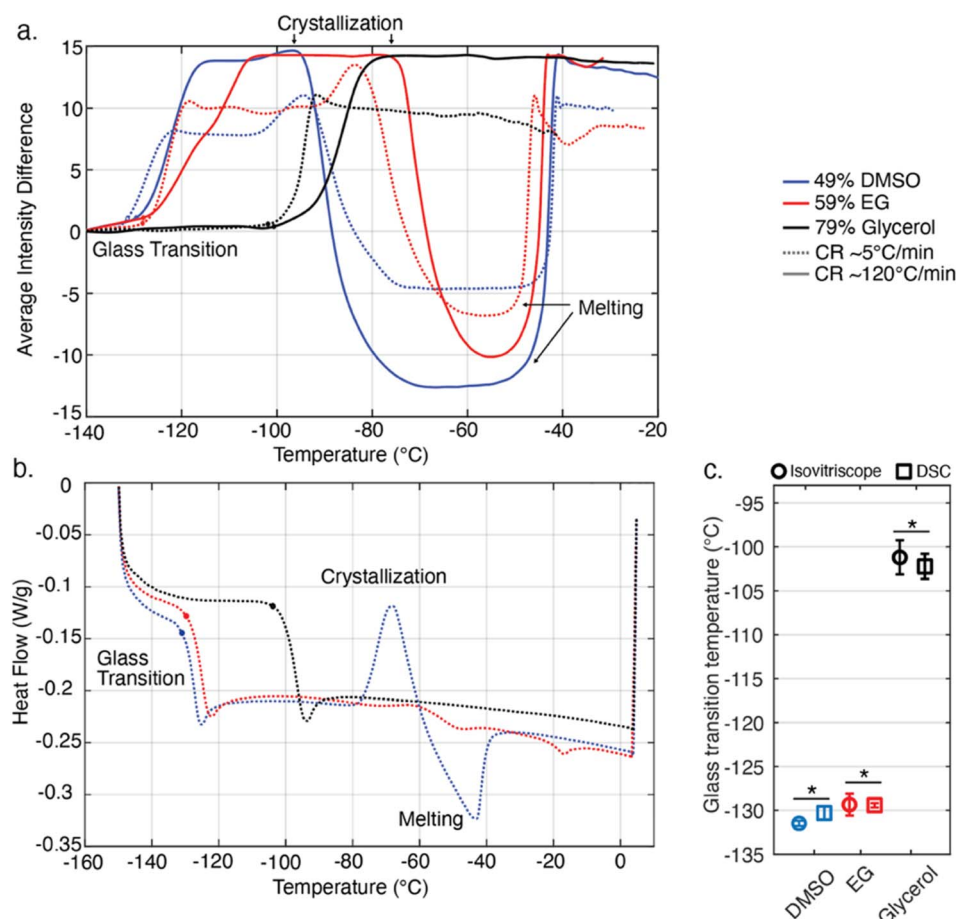

Fig. 7 Results of the constant light intensity (CLI) method and comparison to differential scanning calorimetry (DSC). (a) Intensity–temperature data for three solutions (49% DMSO, 59% ethylene glycol, 79% glycerol) vitrified at two cooling rates ($\sim$200 °C min^{-1} and $\sim$5 °C min^{-1}) and monitored using the CLI method during warming at $\sim$5 °C min^{-1}. (b) DSC curves of the same solutions, cooled and warmed at 5 °C min^{-1}. Relevant phase transition regions are labeled in both panels, and extracted onset glass transition temperatures are marked by circles. (c) Comparison of onset glass transition temperatures between techniques. Markers show the mean value across $n = 3$ replicates, and error bars mark standard deviation. Asterisks mark groups for which ANOVA produced statistical difference ($p > 0.05$).

determined by identifying the point where there is a significant change in the tangent slopes of the curve. Additional details regarding the process can be found in the ESI (ESI Note 2).† For consistency we also apply this approach to extracting the same onset glass transition temperature from the DSC data shown in Fig. 7b, but we note that solution to solution, the thresholding value requires adjustment for the intensity data, but not for DSC. We attribute this to the significantly noisier data produced by the isovitriscope (a ~$500 USD prototype device) as compared to the DSC (a ~$50,000 USD precision metrology product), but anticipate that with superior control of environmental light, alternative sample volumes/geometries, and/or more sophisticated data normalization processes, the T_g extraction process could be streamlined.

Extracted T_g values are marked by circles on Fig. 7a and b for both isovitriscope and DSC data, and average values across triplicate slow cooling trials for each solution are plotted in Fig. 7c, with error bars indicating standard deviation and groupings marked by an asterisk sharing statistical similarity per one-way ANOVA ($p > 0.05$). All extracted T_g values are also tabulated in ESI Note 4,† alongside comparison to literature values. We note a few salient observations: first, in Fig. 7a, it can be seen that the isovitriscope captures the expected trend in onset glass transition temperature with cooling rate, transitioning at marginally warmer temperatures for faster cooling rates.[35] Second, isovitriscope analysis and DSC provide statistically similar values for the onset T_g, with similar standard deviations (~±1–2 °C). Finally, while we do not analyze the melting point here (because we are not monitoring pressure, which may or may not develop upon formation during vitrification processes under isochoric conditions[7,12,18]), we note anecdotally that the labeled melting regions in Fig. 7a align generally with published values for the atmospheric-pressure melting points of 59% ethylene glycol[36] and 49% DMSO.[25] While this work aims only to demonstrate the range of basic capabilities of the isovitriscope, we suggest that future refinement of the platform may enable extraction of glass transition temperatures, crystallization temperatures, and melting temperatures alike.

Conclusion

The isochoric vitrification cryo-macroscope ("isovitriscope") is introduced as an inexpensive and data-rich metrological platform with which to interrogate low-temperature aqueous phase change phenomena in bulk-volume samples, with particular emphasis on the glass transition. The results provided herein aim to illustrate the capabilities of the technique on a proof-of-concept basis, and suggest several avenues of future research related both to the underlying metrology and the science of isochoric vitrification. However, several key limitations of the current device embodiment should be addressed.

First, the device at present does not include active temperature control during cooling and warming, and as such, is limited to cooling and warming rates that may be achieved passively by manipulation of thermal insulation around the chamber. While this is advantageous from a cost and simplicity perspective, future integration of active cooling or heating

elements may enable more granular interrogation of rate effects, in addition to monitoring during the cooling & warming processes (instead of exclusively warming). Observation of the cooling process may lend valuable additional insight into the cavity formation process, which to our knowledge has not yet been directly observed (including by X-ray) in an isochoric vitrification system.

Second, the device at present does not include pressure monitoring. As discussed variously in recent literature, during isochoric vitrification, enhanced pressures are avoided, and thus do not confound measurement of the glass transition temperature.[12,19] However, upon crystallization during rewarming, depending on the thermovolumetric evolution of the system,[18] positive pressures may develop, which, if unaccounted for, may confound attempts to measure the solution melting point based on the intensity output. Furthermore, combined active cooling and pressure monitoring could enable first-of-its-kind optical interrogation of pressurized isochoric glass formation/phase change processes.

Finally, it should be noted that the internal geometry of the chamber represents a significant lever with which to tailor the isovitriscope technique to applications of interest. For example, at the current 2 mL volume scale and 12.7 mm internal diameter, phenomena relevant to practical isochoric vitrification applications[12] may be examined, and in principle, a biological sample could be monitored within. Alternatively, for clearer examination of cracking behaviors, a sample aspect ratio more closely approaching the 2D may be appropriate. For each hypothetical geometry however, the general metrology approach demonstrated here should remain applicable, suggesting the potential for alternative isovitriscope configurations that may power more granular investigation of specific phenomena of interest.

In summary, this work demonstrates an inexpensive new optical metrology platform with which to interrogate the glass transition and other phase change phenomena in aqueous solutions. These findings shed light on a small selection of the many interesting phenomena that occur during isochoric or volumetrically confined vitrification processes. The study demonstrates both qualitative and quantitative data streams that are accessible to the device. Based on these results, we expect that further improvements to the platform and techniques presented in this study may provide significant new insight into low-temperature aqueous phase change phenomena, particularly isochoric vitrification processes.

Methods

Given the focus of this work on the platform and method itself, relevant methodological details are provided throughout the main text above. Where additional detail is necessary to facilitate reproduction, it is included below and in the ESI.†

Solution preparation

All chemicals were sourced from Sigma Aldrich, and all solutions were prepared on a mass/mass basis in de-ionized water.

Solutions were briefly ultrasonicated at room temperature prior to use to remove excess dissolved gases and errant air bubbles.

DSC measurements

Differential scanning calorimetry (DSC) measurements were conducted using a Q2000 series device from TA Instruments. Using samples from the same solution batches employed in the isovitriscope trials, 15 mg samples were transferred *via* micropipette to Tzero-brand aluminum hermetic DSC pans, which were then lidded and sealed using a Tzero press. The temperature was then cycled from room temperature to -150 °C at cooling and warming rates of 5 °C min^{-1}. Onset glass transition temperatures were extracted in accordance with standard ASTM E1356-08, using the method described in ESI Note 2.†

Statistical analysis

The statistical analysis shown in Fig. 6c was conducted using the *anova1()* function in MATLAB 2023a, with an alpha value of 0.05 defining the threshold for statistical significance.

Data availability

All MATLAB scripts and data used for the research herein are available upon reasonable request to the authors.

Author contributions

MPP conceived and supervised the study. SK and FV designed and constructed the isochoric chamber. SK and RS designed and constructed the optical platform, with assistance from CA and GA, and conducted the experiments. SK performed the glass transition temperature analyses. HS performed the DSC experiments. SK, RS, and MPP wrote the manuscript and created the figures, and CA and GA edited the manuscript. All authors approved the final version.

Conflicts of interest

The authors declare no competing interests.

Acknowledgements

References

1 J. Dubochet, M. Adrian, J. J. Chang, J. C. Homo, J. Lepault, A. W. McDowall, *et al.*, Cryo-electron microscopy of vitrified specimens, *Q. Rev. Biophys.*, 1988, **21**(2), 129–228.

2 G. M. Fahy and B. Wowk, *Principles of Cryopreservation by Vitrification*, 2015, pp. 21–82.

3 S. Giwa, J. K. Lewis, L. Alvarez, R. Langer, A. E. Roth, G. M. Church, *et al.*, The promise of organ and tissue preservation to transform medicine, *Nat. Biotechnol.*, 2017, **35**(6), 530–542.

4 Z. Han, J. S. Rao, L. Gangwar, B.-E. Namsrai, J. L. Pasek-Allen, M. L. Etheridge, *et al.*, Vitrification and nanowarming enable long-term organ cryopreservation and life-sustaining kidney transplantation in a rat model, *Nat. Commun.*, 2023, **14**(1), 3407.

5 P. G. Debenedetti and F. H. Stillinger, Supercooled liquids and the glass transition, *Nature*, 2001, **410**(6825), 259–267.

6 P. Lunkenheimer, A. Loidl, B. Riechers, A. Zaccone and K. Samwer, Thermal expansion and the glass transition, *Nat. Phys.*, 2023, **19**(5), 694–699.

7 P. K. Solanki and Y. Rabin, Perspective: Temperature-Dependent Density and Thermal Expansion of Cryoprotective Agents, *Cryoletters*, 2022, **43**(1), 1–9.

8 Z. Han, L. Gangwar, E. Magnuson, M. L. Etheridge, C. O. Pringle, J. C. Bischof, *et al.*, Supplemented phase diagrams for vitrification CPA cocktails: DP6, VS55 and M22, *Cryobiology*, 2022, **106**, 113–121.

9 A. Sharma, J. S. Rao, Z. Han, L. Gangwar, B. Namsrai, Z. Gao, *et al.*, Vitrification and Nanowarming of Kidneys, *Adv. Sci.*, 2021, **8**(19), 2101691.

10 G. M. Fahy, D. R. MacFarlane, C. A. Angell and H. T. Meryman, Vitrification as an approach to cryopreservation, *Cryobiology*, 1984, **21**(4), 407–426.

11 L. Zhan, M. Li, T. Hays and J. Bischof, Cryopreservation method for Drosophila melanogaster embryos, *Nat. Commun.*, 2021, **12**(1), 2412.

12 M. J. Powell-Palm, E. M. Henley, A. N. Consiglio, C. Lager, B. Chang, R. Perry, *et al.*, Cryopreservation and revival of Hawaiian stony corals using isochoric vitrification, *Nat. Commun.*, 2023, **14**(1), 4859.

13 A. Chiu-Lam, E. Staples, C. J. Pepine and C. Rinaldi, Perfusion, cryopreservation, and nanowarming of whole hearts using colloidally stable magnetic cryopreservation agent solutions, *Sci. Adv.*, 2021, **7**(2), eabe3005.

14 D. Lilley, J. Lau, C. Dames, S. Kaur and R. Prasher, Impact of size and thermal gradient on supercooling of phase change materials for thermal energy storage, *Appl. Energy*, 2021, **290**, 116635.

15 A. N. Consiglio, Y. Ouyang, M. J. Powell-Palm and B. Rubinsky, An extreme value statistics model of heterogeneous ice nucleation for quantifying the stability of supercooled aqueous systems, *J. Chem. Phys.*, 2023, **159**(6), 064511.

16 P. K. Solanki and Y. Rabin, Is isochoric vitrification feasible?, *Cryobiology*, 2023, **111**, 9–15.

17 J. T. Parker, A. N. Consiglio, B. Rubinsky and S. A. Mäkiharju, Direct comparison of isobaric and isochoric vitrification of two aqueous solutions with photon counting X-ray computed tomography, *Cryobiology*, 2024, **114**, 104839.

18 S. Kavian and M. J. Powell-Palm, Limits of pressure-based ice detection during isochoric vitrification, *Cryobiology*, 2024, 104905.

19 Y. Zhang, G. Ukpai, A. Grigoropoulos, M. J. Powell-Palm, B. P. Weegman, M. J. Taylor, *et al.*, Isochoric vitrification: An experimental study to establish proof of concept, *Cryobiology*, 2018, **83**, 48–55.

20 M. J. Powell-Palm, B. Rubinsky and W. Sun, Freezing water at constant volume and under confinement, *Commun. Phys.*, 2020, **3**(1), 39.

21 A. N. Consiglio, D. Lilley, R. Prasher, B. Rubinsky and M. J. Powell-Palm, Methods to stabilize aqueous supercooling identified by use of an isochoric nucleation detection (INDe) device, *Cryobiology*, 2022, **106**, 91–101.

22 S. I. Câmpean, G. A. Beschea, A. Serban, M. J. Powell-Palm, B. Rubinsky and G. Nastase, Analysis of the relative supercooling enhancement of two emerging supercooling techniques, *AIP Adv.*, 2021, **11**(5), 055125.

23 H. Huang, M. L. Yarmush and O. B. Usta, Long-term deep-supercooling of large-volume water and red cell suspensions *via* surface sealing with immiscible liquids, *Nat. Commun.*, 2018, **9**(1), 3201.

24 G. M. Fahy and B. Wowk, Principles of cryopreservation by vitrification, *Cryopreservation and Freeze-Drying Protocols*, 2015, pp. 21–82.

25 D. H. Rasmussen and A. P. Mackenzie, Phase Diagram for the System Water–Dimethylsulphoxide, *Nature*, 1968, **220**(5174), 1315–1317.

26 D. M. Vispute, P. K. Solanki and Y. Rabin, Large surface deformation due to thermomechanical effects during cryopreservation by vitrification – mathematical model and experimental validation, *PLoS One*, 2023, **18**, e0282613.

27 C. Berrospe-Rodriguez, J. Schwan, G. Nava, F. Kargar, A. A. Balandin and L. Mangolini, Interaction between a low-temperature plasma and graphene: an *in situ* Raman thermometry study, *Phys. Rev. Appl.*, 2021, **15**(2), 024018.

28 I. Đuričković, R. Claverie, P. Bourson, M. Marchetti, J. M. Chassot and M. D. Fontana, Water–ice phase transition probed by Raman spectroscopy, *J. Raman Spectrosc.*, 2011, **42**(6), 1408–1412.

29 K. Rolle, K. Okotrub, E. Evmenova, A. Kuznetsov, S. Babin and N. Surovtsev, Reversal of crystallization in cryoprotected samples by laser editing, *J. Chem. Phys.*, 2024, **160**(18), 184506.

30 S. Rodrigues, C. A. Alves, A. Cavaleiro and S. Carvalho, Water and oil wettability of anodized 6016 aluminum alloy surface, *Appl. Surf. Sci.*, 2017, **422**, 430–442.

31 A. Surtaev, V. Serdyukov, J. Zhou, A. Pavlenko and V. Tumanov, An experimental study of vapor bubbles dynamics at water and ethanol pool boiling at low and high heat fluxes, *Int. J. Heat Mass Transfer*, 2018, **126**, 297–311.

32 H. Zhang, J. Gottberg and S. Ryu, Contact angle measurement using a Hele-Shaw cell: A proof-of-concept study, *Results Eng.*, 2021, **11**, 100278.

33 Y. Rabin, Mathematical modeling of surface deformation during vitrification, *Cryobiology*, 2021, **102**, 34–41.

34 L. E. Ehrlich, J. S. G. Feig, S. N. Schiffres, J. Malen and Y. Rabin, Large Thermal Conductivity Differences between the Crystalline and Vitrified States of DMSO with Applications to Cryopreservation, *PLoS One*, 2015, **10**(5), e0125862.

35 A. D. Bravenec and D. C. Catling, Effect of Concentration, Cooling, and Warming Rates on Glass Transition Temperatures for $NaClO_4$, $Ca(ClO_4)_2$, and $Mg(ClO_4)_2$ Brines with Relevance to Mars and Other Cold Bodies, *ACS Earth Space Chem.*, 2023, **7**(7), 1433–1445.

36 D. R. Cordray, L. R. Kaplan, P. M. Woyciesjes and T. F. Kozak, Solid-liquid phase diagram for ethylene glycol + water, *Fluid Phase Equilib.*, 1996, **117**(1–2), 146–152.